Biotechnological Communication

BBRC Bioscience Biotechnology Research Communications

Biosc.Biotech.Res.Comm. Vol 13 No (4) Oct-Nov-Dec 2020 Pp 1954-1961

Inhibition Kinetics of Immobilized Cathepsin B on the Surface of Gold Nanoparticles

Iram Wahid[1], A.N. Muhammad Zafar Iqbal[2] and Mohd Sajid Khan*[1]

[1]*Department of Biosciences, Integral University, Lucknow 226026, India*

[2]*Department of Studies in Zoology, Government First Grade UG & PG College, Karwar 581301, India*

ABSTRACT

Present study is based on the concept of green synthesis of gold nanoparticles using cathepsin B and functionalization of cathepsin B on their surface which are involved in cancer. Classical citrate method was used to reduce chloroauric acid with tri-sodium citrate in an aqueous solution to produce citrate gold nanoparticles (C-GNPs). Further, these nanoparticles were immobilized with cathepsin B in order to study the conformation changes during and after function alization. The C-GNPs and cathepsin B immobilized gold nanoparticles (Cat-B-GNPs) were characterized by UV-VIS spectroscopy, TEM, DLS, Zeta potential, SEM and FTIR to confirm the size, functional group interactions, production, stability, crystalline nature, size and shape distribution. However, FTIR studies confirmed the attachment of cathepsin B in the gold nanoparticles. The variation in 2D and 3D conformation of cathepsin B during immobilization was studied by Circular Dichroism and Fluorescence spectroscopy, respectively. It was observed that total changes in α- helix, stand, and turn is 45.41%, 34.75%, 76%, respectively. After immobilization, a 54.91% changes in tertiary structure was found. The change in 2D & 3D conformation of cathepsin B after immobilization may improve cathepsin B potency which would be verified by enzyme kinetics inhibition. Results showed that E-64 significantly inhibited Cat-B-GNPs activity with an IC_{50} of 4.88 µM and inhibition was a non-competitive type of inhibition with a K_i of 5.09 µM. Michaelis-Menten constant K_m of cathepsins B and Cat-B-GNPs were determined by using Z-Phe-Arg-AMC as substrates and E-64 as a model inhibitor.

KEY WORDS: CATHEPSIN B, CIRCULAR DICHROISM, E-64, GOLD NANOPARTICLES, Z-PHE-ARG-AMC.

INTRODUCTION

In malignant tumors, the expression of cathepsin B is highly upregulated and secreted into the extracellular environment (Jakoš et al., 2019) that are required for cancer progression (Poreba et al., 2019) Overexpression of cathepsin B has been demonstrated in various types of cancers, including breast cancer, glioma, melanoma, and oesophageal, pancreatic, colon, renal and prostate cancer. These endogenous tumour specific characteristics provide valuable tools for the design of formulations that will only be activated in the tumour microenvironment (Mijanovic, et al., 2019). Cathepsins act on the drug release process from the nanomaterials. Drug release behaviour studies with nanoparticles showed that the nanoparticles had the greatest release of contents in the presence of cathepsin B at lysosomal pH, indicating the requirement of cathepsin B cleavage for sufficient drug delivery.

There have been various nanoparticles based delivery strategies have been developed such as rotaxane modified mesoporous silica nanoparticles to improve targeting of anticancer drug doxorubicin (Anderson et al., 2017), PEGylated PLGA nanoparticles encapsulated paclitaxel

Article Information:
Corresponding author email: *research.sajid@gmail.com*
Received 26/10/2020 Accepted after revision 18/12/2020
P-ISSN: 0974-6455 E-ISSN: 2321-4007
Thomson Reuters ISI Clarivate Analytics
Web of Science ESCI Indexed Journal

Identifiers & Pagination:
Vol 13(4) E-Pub 31st Dec 2020 Pp- 1954-1961

Published by Society for Science & Nature India
DOI: *http://dx.doi.org/10.21786/bbrc/13.4/48*

and etoposide used in cancer (Wang et al., 2015), camptothecin containing nanoparticle drug conjugated with bevacizumab against renal cell carcinoma (Voss et al., 2017), methoxy-poly (ethylene glycol) aldehyde conjugated with doxorubicin and Curcumin against HepG-2 cancer cells (Zhang et al., 2016) and doxorubicin carbonane conjugated polymeric nanoparticles used for cancer therapy (Hejian et al., 2015).

Dendrimer methoxy polyethylene glycol which conjugated with doxorubicin using cathepsin B responsive drug to target cancer cells (Ahn et al., 2009). M.K shim et al developed carrier free nanoparticles of cathepsin B cleavable peptide Phe-Arg-Arg-Gly conjugated with doxorubicin to target cathepsin B (Shim et al., 2019). The concept of using nanoparticles as a carrier for anticancer agents is based on the observation that drugs appear to be inactive while bound onto nanoparticle surface and they elicit their cytotoxic action once the nanoparticles digested within the tumour microenvironment (Li et al., 2000; Rudzicska et al., 2020). Nanoparticle delivery of specific cathepsin inhibitors can enable targeted recognition of cancer cells and effective inhibition of intracellular activity of cathepsins.

PEGylated liposomes with an epoxide based cathepsin B inhibitor NS-629 conjugated through a lipid linker (LNC-NS-629) used in Cathepsin B targeted delivery of therapeutics or diagnosis to the cancer site (Farooq et al., 2018). Poly-lacto-co-glycolic acid (PLGA) nanoparticles and chitosan nanoparticles conjugated with cystatin were successfully developed using an optimized method that retains the inhibitory activity of the encapsulated cystatin. Similarly, PEGylated liposomes conjugated with irreversible epoxyketone cathepsin inhibitors Carfilzomib and bortezomib were successfully developed to target cancer (Stern et al., 2008; Deng et al., 2020).

Cathepsins inhibitor have been shown to be effective anticancer therapeutic agents and delivery with nanoparticle systems can substantially improve their bioavailability, increase circulation time and achieve specific accumulation in tumor tissues. Enzyme inhibition has always been an important field of study, not only because of its usefulness in providing valuable information on fundamental aspects of enzymatic catalysis and metabolic pathways, but also for its implications in pharmacology and toxicology. Compared to reversible inhibition, the kinetics of irreversible inhibition has received relatively little attention. However, it is well established that irreversible modification of enzyme activity is important for studies on the nature of functional groups essential to enzymatic catalysis; such studies cannot be conducted with reversible inhibitor.

In the study presented here, we synthesized citrate mediated gold nanoparticles which functionalized with cathepsin B. The main goal of the study is to detect the unfolding and folding pathway of cathepsin B during the synthesis of Cat-B immobilized GNPs (Cat-B-GNPs). The characterization of C-GNPs and Cat-B-GNPs was done by UV-VIS spectroscopy, TEM, DLS, Zeta potential, SEM and FTIR. Furthermore, the enzyme inhibition kinetics was done to evaluate the efficacy of free enzyme against immobilized enzyme (Cat-B-GNPs) using Z-Phe-Arg-AMC substrate and E-64 as a model inhibitor.

MATERIAL AND METHODS

Tetrachloroauric [III] acid [$HAuCl_4$] was procured from sigma Aldrich Co. USA. Cathepsin B from human liver, the irreversible inhibitor E-64 [L-3-carboxy-trans-2,3-epoxypropionyl- leucylamido-(4-guanidino) butane] and the fluorogenic amido methyl coumaryl substrate Z-Phe-Arg-AMC were purchased from Merck. DTT (dithiothreitol), tri-sodium citrate andEDTA were purchased from HiMediaLaboratories, Mumbai, India. All other reagents were of highest analytical grade available. Active forms of cathepsin B were stored at 4°C in 50 mM sodium acetate buffer (pH 5.0) containing 10 mM methyl methane-thiosulfonate.

In vitro synthesis of citrate encapsulated gold nanoparticles (C-GNPs): In vitro production of C-GNPs was done by reduction of tetra chloroauric [III] acid $HAuCl_4$ with tri-sodium citrate (NaCt) following Turkevich method (Turkevichet al., 1951). Citrate mediated synthesis of GNPs was performed by incubating1mM HAuCl4 with 1% tri-sodium citrate solution in 5ml double distilled water at 100 on a hot plate with continuous stirring at 350 rpm until homogenous solution achieved. C-GNPs gradually produce as the NaCt reduces the gold ion (Au^{3+}) into the gold atom (Au^0). The confirmation of synthesis of C-GNPs was authenticated with change in color of reaction from transparent to light yellow, to grey, purple and then eventually in deep ruby red for gold nanoparticles. Confirmation of synthesis of C-GNPs was confirmed by the UV absorption spectroscopy, TEM, DLS, Zeta potential and SEM. After the completion of the reaction, the reaction mixture was removed from hot plate and air cooled at RT.

Immobilization of cathepsin B over the surface of C-GNPs: Immobilization of cathepsin B over the surface of C-GNPs was done by incubating 33µg/ml with 1ml C-GNPs for 2 hours at room temperature and subsequently, 0.05M of NaCl to the reaction mixture and incubating for 1hour, to increase ion concentration in the solution. CathepsinB immobilized on the surface of GNPs during the transfer of citrate to the NaCl, which prevents the aggregation of GNPs and ensure stability. After the reaction completion, 50% v/v of ethanol treatment was used to remove unbound cathepsin B, and further by centrifugation (10 min) nanoparticles were collected and used further for characterization (Iram et al., 2019).

Characterization of in vitro synthesized C-GNPs and cathepsin B capped gold nanoparticles (Cat-B-GNPs): C-GNPs and Cat-B-GNPs were characterized by various techniques, UV–vis spectrophotometer measurements were performed on a Shimadzu dual-beam spectrophotometer (model UV-1601 PC), operated at a resolution of 1 nm. Transmission electron microscopy (TEM) was done on TecnaiTMG2Spirit BioTWIN FEI Company operated at an accelerating voltage of 80 kV. The sample was prepared by drying a drop of Cat-B-GNPs solution on carbon coated TEM copper grids followed by measurements on TEM.Scanning electron microscopy (SEM) analysis of synthesized Cat-B-GNPs was operated by the use of a Sigma, Zeiss HR-SEM machine. The mean particle size of Cat-B-GNPs was measured with a dynamic light scattering (DLS) particle size analyzer (Zeta Sizer Nano-ZS, Model ZEN3600, Malvern Instrument Ltd).

The particles were sonicated by using Sonic & Material Inc., at 30 W for 1 min. Mean particle size was the average of triplicate measurements for a single sample. The surface charge of C-GNPs and Cat-B-GNPs were measured using a Zeta Sizer Nano-ZS, Model ZEN3600. The confirmation of binding and secondary structure of cathepsin B at the surface of GNPs was done by Fourier transform infrared spectroscopy (FTIR). FTIR spectra of the sample were recorded on a Shimadzu FTIR-8201 PC instrument operated in the diffuse reflectance mode at a resolution of 4 cm^{-1}. To obtain good signal-to-noise ratios, were taken in the range 400–4000 cm^{-1}.

Circular dichroism (CD) Studies: Conformational changes in the secondary structure of cathepsin B due to immobilization over the surface of C-GNPs were performed on a Jasco J 800spectropolarimeter using a 1 mm path length cell. The machine was aligned with D-10-camphorsulfonic acid. The nitrogen flow was fixed at 10 liters/min. The CD spectrum was monitored over a variable wavelength scan (200-250nm). The CD in millidegree obtained over the wavelength range of 190 to 250 nm was converted to mean residue ellipticity (MRE,) using the following conversion: MRE = CD (in mdeg)/cpnl, where cp is molar concentration of protein, n is number of amino acid residues in the protein,and l is path length (in mm).Native and Cat-B-GNPs samples were put in 1 mm path length cuvette and spectra were captured in the variable wavelength scan (200 to 250 nm). Every spectrum was the mean of 3 scans and was recorded at an interval of 1 nm wavelength. The enzyme concentration in these tests was 33µg/ml.

Study of conformational changes in cathepsin B by spectrofluoremeter: 3D Conformational changes in the cathepsin B during immobilization over the surface of C-GNPs were performed on Agilent Carry Eclipse Fluorescence Spectrophotometer–MY16040008 using the FLR software provided by the manufacturer. The fluorescence emission was recognized in the range of wavelength 300-400nm after exciting the protein at 280nm. Both the excitation and emission silt width were set at 5nm & voltage is 600 V. The excitation & emission spectra were smoothed with Savitzky-Golay smoothing factor 10. Percent changes in fluorescence intensity (FI) of cathepsin B during immobilization was calculated from the following equation: % changes in FI = [(FI of native cathepsin B – FI of cathepsin B with GNPs at different time)/FI of native cathepsin B] × 100.

Enzymatic activity of Cat-B-GNPs against Fluorogenic methyl coumaryl substrate (Z–Phe–Arg–AMC): Standard conditions used to determine the hydrolytic activity of cathepsin B (at pH 6.5), against the fluorogenic substrate Z–Phe-Arg–AMC (stock solutions prepared in dimethyl sulfoxide) at 37°C according to the method of Barrett and Kirschke (Barrettet al., 1988). After 30 min of incubation with substrates, the hydrolytic reaction by this proteinase was terminated by adding 5% of TCA (trichloro acetic acid) containing 2.5 ml HCl. The intensity of fluorescence of the mixture was measured at an excitation wavelength of 350 nm and an emission wavelength of 420 nm. One unit of enzyme activity was expressed as the amount of enzyme that can hydrolyze methyl coumaryl amide substrates and release1 µmol of amino methyl coumarin within 1 min of reaction at 37°C.

For the Lineweaver–Burk analysis, Cat-B-GNPs (250ng/ml) was incubated with inhibitor at 12µM and 24µM assayed at increasing concentrations of substrate (10µM, 20µM, 30µM,40 µM) in 50 mM sodium potassium phosphate buffer (pH 6.5) containing 2 mM EDTA and 4mM DTT was separately added. The fluorescent intensity of free amino methyl coumarin release from the hydrolysis of methyl coumaryl amide substrate due to this proteinase was measured continuously by a fluorescence spectroscopy (excitation, 350 nm; emission, 420 nm; slit, 5 nm) at 37°C. The initial velocities (v) were calculated from the reaction curve, i.e. the slop of the initial linear cure. Lineweaver-Burk doublereciprocalplot of substrate concentration (s) versus initialvelocity (v) was used to calculate the Michaelis constant (K_m) and maximum velocity (V_m).

RESULTS AND DISCUSSION

Preparation of C-GNPs and Characterization: A typical citrate reduction method of gold nanoparticles at 100 takes 30-40 minutes for the characteristic ruby red color to appear in the solution. Three different aspects are of crucial importance for obtaining desirable size of nanoparticles (i) the temperature, (ii) the pH, and (iii) concentration of Au atoms (Ojea-Jiménez et al., 2009). The synthesis of C-GNPs was confirmed by a gradual transform in color starting from light grey to

characteristic ruby red color subsequent by incubation of citrate and Au atom. The transformation in color is due to the surface plasmon resonance of C-GNPs. Further, it was confirmed by UV-Visible spectroscopy, the absorption band of C-GNPs showed an intense peak at 522nm (Fig. 1a) (Sakellari, et al 2020).

Figure 1: Characterization of C-GNPs under (a) UV–vis spectroscopy (b) Transmission electron microscopy (c) Dynamic light scattering (d) Zeta potential and (e) Scanning electron microscopy

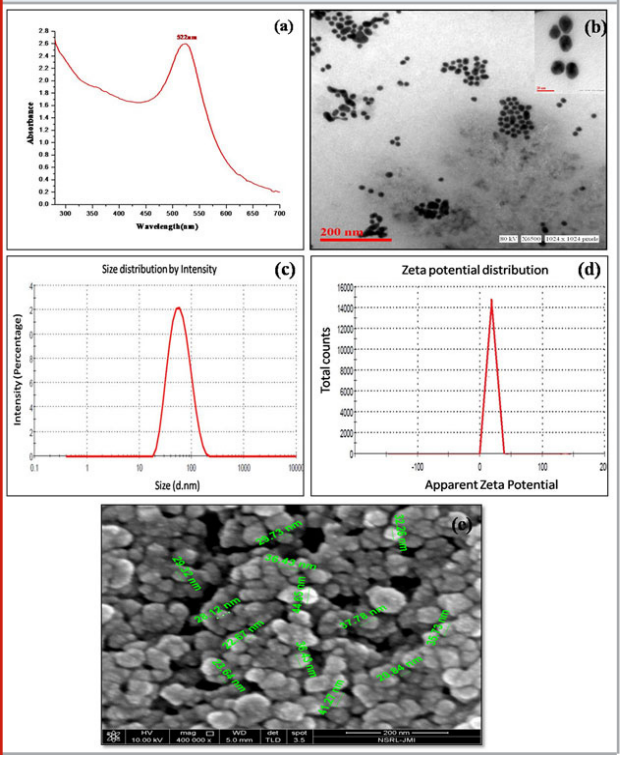

High resolution images of C-GNPs were obtained using TEM and most particles were estimated to be monodispersed and spherical at an average size of approximately ~18 nm (Fig.1b). In addition, DLS was carried out to estimate the hydrodynamic radius of C-GNPs was obtained to be 49.53 nm (Fig.1c). C-GNPs with a negative charge were found to be stable and their zeta potential values were found to be -1mV (Fig. 1d). SEM image clearly shows the spherical and uniformly distributed C-GNPs (Fig.1e).

Immobilization of cathepsin B on C-GNPs and their characterization: Electrostatic repulsion between negatively charged cathepsin B and negatively charged spherical C-GNPs should hinder the protein adsorption. However, in the present study strong interaction was observed. The strong binding of cathepsin B to nanoparticle surface occurred most probably due to the NaCl, which start dislocation of citrate ions towards the Na ion. Cathepsin B, a strong stabilizing agent with Cys, Asp and His in the active site which makes nanoparticle more stable and prevent aggregation. Immobilization process of cathepsin B on the surface of GNPs is spontaneous process where most of type interactions involve such as hydrophobic interaction, and ionic interaction. Hydrophobic interactions are due to attraction between hydrophobic parts of the cathepsin B and the gold surface resulting, the formation of non-covalent bond. Ionic interaction are formed between positively charged amino acid and negatively charged gold nanoparticle surface.

Figure 2: Characterization of Cat-B-GNPs under (a) UV–vis spectra (b) Transmission electron microscopy (c) Zeta potential (d) DLS (e) Scanning electron microscopy and (f) FTIR

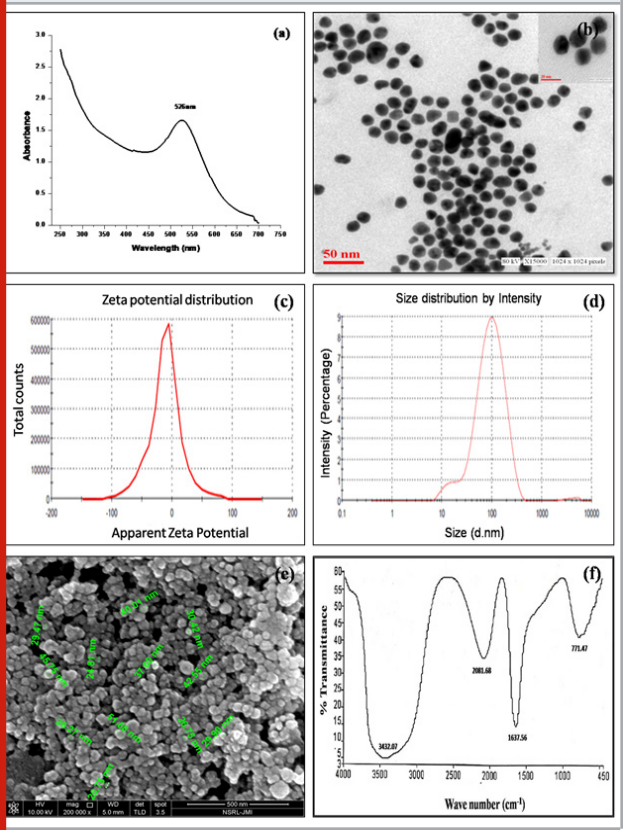

Cathepsin B stabilized/immobilized GNPs (Cat-B-GNPs) have shown a decrease in intensity of the peak with a noticeable red shift from 522 nm to 526 nm in comparison to C-GNPs (Fig. 2a). The red shift in SPR confirms a change in the surface chemistry of C-GNPs due to immobilization of cathepsin B on their surface. Generally, GNPs single absorption peak in the visible range between 512-550 nm, because of surface Plasmon resonance display and show heavy absorption of visible light at 520 nm. TEM is another important aspect for characterization shows the high resolution TEM image of Cat-B-GNPs. The size of Cat-B-GNPs has been determined by measuring the diameter of whole particles on TEM images.

TEM calculates the size of nanoparticles by directly transmitted electrons which give the information about only inorganic core and doesn't include hydration layer. High resolution images of Cat-B-GNPs were obtained using TEM and most particles were estimated to be monodispersed, spherical and evenly dispersed at an average size of approximately ~20 nm (Fig. 2b). Their shapes were found to be spherical and monodispersion state, this is because of negatively charged layer of cathepsin B, which repel from each other. The cathepsin B molecules adsorb onto the surface of the C-GNPs and make a layer of negatively charged ions. The resulting electrostatic interaction provides an interparticle force strong enough for the particles to stay separated.

The concentration, distribution, ionization, exposure of charged moieties, adsorption of the particles can be recorded by zeta potential. The change in zeta potential of Cat-B-GNPs was observed and it was found to be –11.4 mV (Fig. 2c). Further, DLS was conducted to estimate the hydrodynamic radius of Cat-B-GNP was found to be 77.29 nm (Fig. 2d). SEM results revealed that the particles are smaller in size and uniformly distributed. However, the particle size of the Cat-B-GNPs was estimated to be in the range of 25-35nm (Fig. 2e).

In order to detect involvement of different functional groups of protein to functionalize GNPs, FTIR was carried out (Fig. 2f). There are two regions 1700–1600 cm^{-1} 1550–1500 cm-1 in the spectrum, which are unique to the protein secondary structure, called as amide I and II bands. These provide valuable information on conformational changes of the protein when immobilized with the nanoparticles. The amide I band (C=O stretch) has a correlation with the secondary structure of protein. The immobilization of cathepsin B over C-GNPs was confirmed by observing a characteristic peak at 1637.56cm-1corresponding to the presence of amide groups.

Further smaller peak observed at 771.47cm-1 correspond to C-N of aliphatic amines stretch of peptide bond also confirms the immobilization. In this study a novel method has been developed to immobilize cathepsin B over gold nanoparticles surface. During immobilization over the surface of gold nanoparticles cathepsin B undergo several changes in their secondary and tertiary structure and then finally adopts its native structure with less variations which do not alter cathepsin B property. Only some reports are presented where the folding & unfolding of protein have been studied using techniques such as circular dichroism (CD) spectroscopy, and fluorescence spectroscopy.

In this study, citrate mediated gold nanoparticles have been stabilized/immobilized by cathepsin B. The CD spectra of cathepsin B show a clear change in the protein structure during immobilization over the surface of GNPs in the far UV region between 200 and 240 nm. A more detailed analysis of the spectrum using K_2D_3 software which allow estimating the percentage of secondary structure in each CD spectrum. The α helical structure of the protein in the far UV region is characterized by negative peaks at 208-210 and 222 nm and positive peaks between 190 and 192 nm. The results were expressed as MRE (mean residue ellipticity) in deg•cm2•$dmol^{-1}$, which is defined as: MRE = θ obs/ (10Cpnl), Where θ obs is the CD in milli degrees, n is the number of amino acid residues, l is the path length of the cell, and Cp is the mole fraction. Helical content of cathepsin B was calculated from the MRE values at 222 nm using the following equation: % α helix = (MRE222 – 2340/30300) × 100.

The structure of cathepsin B is comprised of a helix (14%), β sheets and turns with 35% residual part in various structures (Garnier et al., 1978). The molecular mass of cathepsin B is 38 kDa with three disulfide bridges and a solitary free cysteine amino acid among cumulative 339 amino acids demonstrates the Native and cathepsin B-Gold in far-UV CD spectra (Cavallo-Medved et al., 2011). There was an almost 45.41% in α-helical structure and 34.75% changes observed in -sheet in the secondary structure after immobilization of cathepsin B (Fig. 3).

Figure 3: (a) Far UV-CD spectra of Cathepsin B and Cat-B-GNPs at different incubation period (b) Bar graphs are representing % α-helix & β-sheet content of cathepsin B during immobilization on the surface of GNPs. % α-helix & β-sheet content was interpreted through K2D2 software (http://cbdm-01.zdv.unimainz.de/~andrade/k2d2/). Values (Percentage) are the average of three determinations. Significantly different from native cathepsin B at a p<0.01

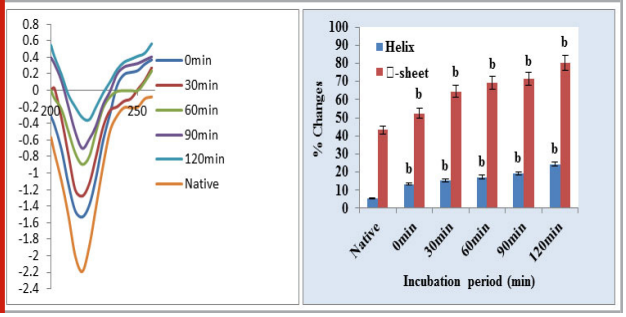

This can be expected to conformational change from the native state of protein after binding to the nanoparticle surface. α helical structure has two negative bands in 210 and 222 nm. With the progress of the reaction (till 2Hrs) ellipticity gradually decreases with time due to the extent of α-helical structure of cathepsin B structure is reduced as a result of immobilization with GNPs. The above information clearly showed that there was a change in 2D conformation of cathepsin B after immobilization over GNPs but 3D conformation didn't alter significantly.

This implies that slight loss in secondary structure does not lead to tertiary structure loss cm^{-1}.

Fluorescence studies: In the beginning of the reaction, very strong fluorescence signal was observed because at the beginning gold was present in the form of Au^{+0} ions and it interacts with cathepsin B through hydrophobic interactions. As the incubation period proceeds (at 30 min), less fluorescence signal was obtained because the exposure of aromatic amino acid gradually decreases which enhance hydrophobic interactions and cause folding of cathepsin B. With the progress of the reaction (till 120min) fluorescence intensity decreases with time due to involvement of hydrophobic sites of cathepsin B in the interaction with GNPs. Ultimately, after completion of the reaction, cathepsin B adopts its native structure (Fig. 4).

Figure 4: (a) Changes in protein fluorescence intensity (fluorescence excitation 280nm) in the Cathepsin B during immobilization at different incubation time (0min, 30min, 60min, 90min, and 120 min). (b) Significantly different from native cathepsin B at a p^a<0.01.Significantly different from native cathepsin B at a pb<0.001

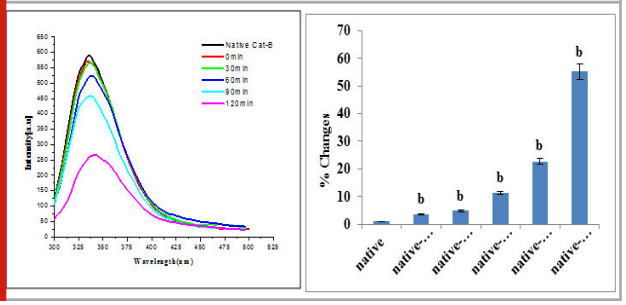

Figure 5: Line weaver–Burk plot of Cat-B-GNPs inhibition by different concentration of E-64 at 37.

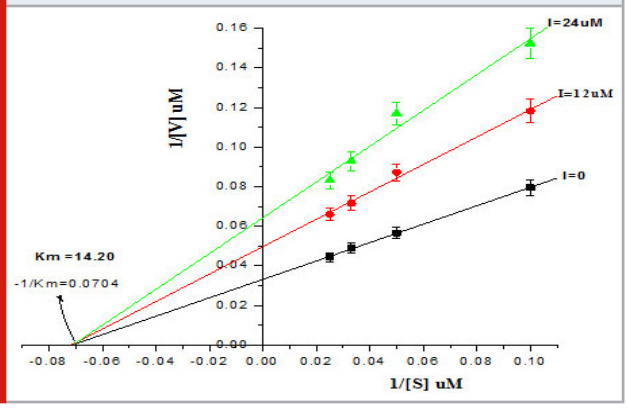

Inhibition Kinetics Studies: The inhibitor kinetics studies were attempted to explain how an inhibitor acts on enzyme and predict its efficacy. The kinetic constants K_m and K_i are critical to understand enzymatic action on controlling metabolism of an organism. We studied enzyme inhibition kinetics of E-64 on Cat-B-GNPs. The Michaelis-Menten constant K_m was determined by Lineweaver-Burk plot in which the reciprocals of substrate hydrolysis (1/V) for inhibitor concentration were plotted against the reciprocals of the substrate concentrations by fitting the resulting data in ORIGIN 6.1 (Fig.5). The K_m value for the both cathepsin B and Cat-B-GNPs with Z-Phe-Arg-AMC substrate was found to be 14.70 µM and 14.20 µM at 37□ (Fig. 6).

Figure 6: Line weaver–Burk plots of both cathepsin B and Cat-B-GNPs to calculate K_m against Z-Phe-Arg-AMC at 37□

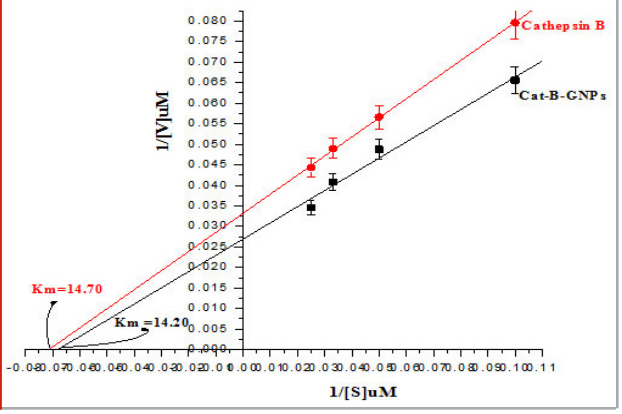

The Cat-B-GNPs activity was measured at different concentrations of substrate Z-Phe-Arg-AMC (10, 20, 30, and 40 µM). The K_m value for the Cat-B-GNPs with Z-Phe-Arg-AMC was found to be 14.20 µM at 37□ (Fig. 5). The reciprocals of substrate hydrolysis (1/v) were plotted against the different enzyme concentrations (Fig.7). The inhibition constant K_i was determined by Dixon method, hydrolytic activity of Cat-B-GNPs were measured in the presence of 10µM and 30µM Z-Phe-Arg-AMC, at increasing concentrations of inhibitor at 37□ for 30 min (Fig. 6). The reciprocals of substrate hydrolysis (1/v) were plotted against the inhibitor concentration and the K_i was determined by fitting the data using ORIGIN 6.1.The double reciprocal Lineweaver Burk Plot demonstrated the non-competitive mode of inhibition of Cat-B-GNPs by E-64, obtained values of Ki from Dixon plot was found to be 5.09 µM (Fig. 8). The E-64 inhibitor was found to inhibit Cat-B-GNPs with an IC_{50} value (50% inhibitory concentration) of 4.88 µM (Fig. 9). The inhibition of Cat-B-GNPs followed a linear pattern with increasing concentrations of the inhibitor.

In the present study, E-64 displayed a significant concentration dependent inhibition of Cat-B-GNPs using Z-Phe-Arg-AMC as a substrate. To elucidate the mechanism of Cat-B-GNPs inhibition by E-64, kinetic studies of enzyme activity were performed. The relationship between substrate concentration and reaction velocity was in good agreement with Michaelis–Menten equation. Hence, the result demonstrated that mechanism

of Cat-B-GNPs inhibition was of non-competitive nature. For the kinetic analysis and rate constant determinations, the assays were carried out in triplicate, and the average value was considered throughout this work.

Figure 7: Linear fit between velocity [v] and enzyme concentration.

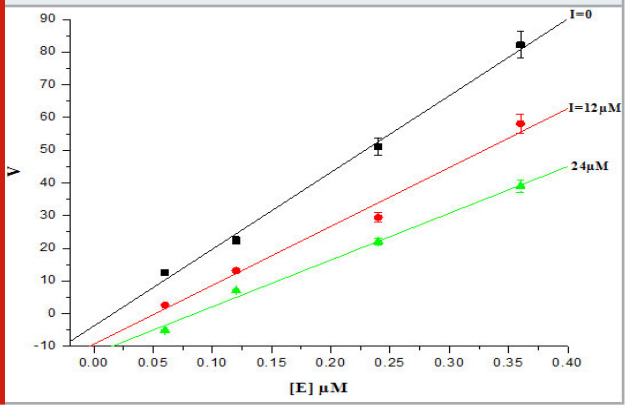

Figure 8: Dixon's Plot: Enzymatic activity of the Cat-B-GNPs was estimated using the substrate Z-Phe-Arg-AMC (10µM and 40µM) at different concentrations of E-64. Reciprocals of the reaction velocity were plotted versus the E-64 concentration. The straight lines indicated the best fit of the data obtained. The inhibition constant K_i was calculated from the intersection point of the two plots.

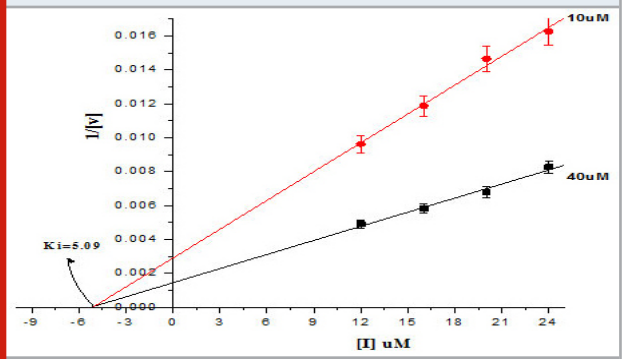

Figure 9: Cat-B GNPs inhibition curve for E-64.

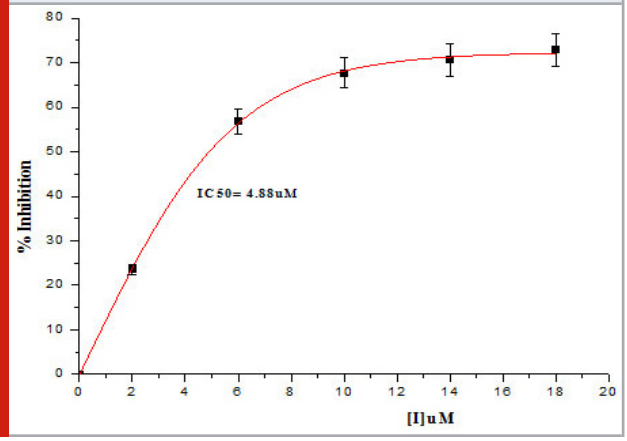

CONCLUSION

The Present study reveals that sodium citrate behaves as a reducing and cathepsin B as a capping agent. After controlled synthesis their physic-chemical characterization is important. It is suggested that for the toxicological studies nanomaterials must have to confirm the crucial set of characteristic which includes size, shape, surface, charge, condition of scattering, chemical composition, surface range and surface chemistry. Surface chemistry of nanomaterial is often another essential step which includes modification of the surface of nanoparticles by using functionalizing/ immobilization. During the process of immobilization, cathepsin B undergoes several stages of unfolding to folding and finally, after complete immobilization on C-GNPs, adopts a final configuration with variations in 3D & 2D structures. Further, we investigated the kinetic mechanism of Cat-B-GNPs and the interaction mechanisms with E-64 inhibitor.

REFERENCES

Ahn, S.J., Browngardt, C.M., Burne, R.A., (2009). Changes in biochemical and phenotypic properties of *Streptococcus mutans* during growth with aeration. Applied and environmental microbiology, 75, pp. 2517-2527.

Anderson, C.F., and Cui, H.,(2017). Protease-sensitive nanomaterials for cancer therapeutics and imaging. Industrial and engineering chemistry research, 56, pp.5761-5777.

Aramwit, P., Bang, N., Ratanavaraporn, J., and Ekgasit, S., (2014). Green synthesis of silk sericin-capped silver nanoparticles and their potent anti-bacterial activity. Nanoscale research letters, 9, p.79.

Barrett, A.J., and Kirschke, H., (1988). Cathepsin B, cathepsin H, and cathepsin L. In Methods in enzymology, 80, pp. 535-561.

Cavallo-Medved, D., Moin, K., and Sloane, B., (2011). Cathepsin B: Basis sequence: Mouse. The AFCS-nature molecule pages, p.2011.

Farooq, M.U., Novosad, V., Rozhkova, E.A., Wali, H., Ali, A., Fateh, A.A., Neogi, P.B., Neogi, A., and Wang, Z., (2018). Gold nanoparticles-enabled efficient dual delivery of anticancer therapeutics to HeLa cells. Scientific reports, 8, p.2907.

Garnier, J., Osguthorpe, D.J., and Robson, B., (1978). Analysis of the accuracy and implications of simple methods for predicting the secondary structure of globular proteins. Journal of molecular biology, 120, pp. 97-120.

Hejian, X., Dongfang, Z., Yanxin, Q., Zhiyun, Z., Zhigang, X., Xuesi, C., Xiabin, J., Fanbo, M., and Yubin, H., (2015). Doxorubicin-loaded carborane-conjugated polymericnanoparticles as delivery system for combination cancer therapy, Biomacromolecules, 16, pp.3980-3988.

Iram, S., Zahera, M., Wahid, I., Baker, A., Raish, M., Khan, A., Ali, N., Ahmad, S., and Khan, M.S., (2019). Cisplatin bioconjugated enzymatic GNPs amplify the effect of cisplatin with acquiescence. Scientific reports, 9, p.13826.

Jakoš, T., Pišlar, A., Jewett, A. and Kos, J., (2019). Cysteine cathepsins in tumor-associated immune cells. Frontiers in Immunology, 10, p.2037.

Lee, G.Y., Qian, W.P., Wang, L., Wang, Y.A., Staley, C.A., Satpathy, M., Nie, S., Mao, H., and Yang, L., (2013). Theranostics nanoparticles with controlled release of gemcitabine for targeted therapy and MRI of pancreatic cancer. ACS nano, 7, pp. 2078-2089.

Li, C., Robert, A.N., Qing, P.W., Shi, K., Wei, C., Toni, H., Zuxing, K., Melvin, D.B., Chusilp, C., and Sidney, W., (2000). Biodistribution of paclitaxel and poly (L-glutamic acid)-paclitaxel conjugate in mice with ovarian OCa-1 tumor. Cancer chemotherapy and pharmacology, 46, pp. 416-422.

Mijanovic, O., Brankovic, A., Panin, A.N., Savchuk, S., Timashev, P., Ulasov, I. and Lesniak, M.S., (2019). Cathepsin B: A sellsword of cancer progression. Cancer letters, 449, pp.207-214.

Ojea-Jiménez, I., and Puntes, V.J., (2009). Instability of Cationic Gold Nanoparticle Bioconjugates: The Role of Citrate Ions. Journal of the American Chemical Society, 131, pp.13320–13327.

Poreba, M., Groborz, K., Vizovisek, M., Maruggi, M., Turk, D., Turk, B., Powis, G., Drag, M. and Salvesen, G.S., (2019). Fluorescent probes towards selective cathepsin B detection and visualization in cancer cells and patient samples. Chemical Science, 10(36), pp. 8461-8477.

Rudzicska, M., Parodi, A., Maslova, V. D., Efremov, Y. M., Gorokhovets, N. V., Makarov, V. A., and Zamyatnin, A. A., (2020). Cysteine Cathepsins Inhibition Affects Their Expression and Human Renal Cancer Cell Phenotype. Cancers, 12, p.1310.

Sakellari, G.I., Hondow, N., and Gardiner, P.H., (2020). Factors Influencing the Surface Functionalization of Citrate Stabilized Gold Nanoparticles with Cysteamine, 3-Mercaptopropionic Acid or l-Selenocystine for Sensor Applications. Chemosensors, 8, p.80.

Shim, M.K., Park, J., Yoon, H.Y., Lee, S., Um, W., Ki and Byun, Y., (2019). Carrier-free nanoparticles of cathepsin B-cleavable peptide-conjugated doxorubicin prodrug for cancer targeting therapy. Journal of controlled release, 294, pp.376-389.

Stern, J.M., Stanfield, J., Kabbani, W., Hsieh, J.T., and Cadeddu, J.A., (2008). Selective prostate cancer thermal ablation with laser activated gold nanoshells. The journal of urology, 179, pp.748-753.

Turkevich, J., Stevenson, P.C., and Hillier, J., (1951). A study of the nucleation and growth processes in the synthesis of colloidal gold. Discussion of the faraday society, 11, pp.55-75.

Voss, M.H., Hussain, A., Vogelzang, N., Lee, J.L., Keam, B., Rha, S., Vaishampayan, U., Harris, W.B., Richey, S., Randall, J.M., and Shaffer, D., (2017). A randomized phase II trial of CRLX101 in combination with bevacizumab versus standard of care in patients with advanced renal cell carcinoma. Annals of oncology, 28, pp.2754-2760.

Wang, B., Yu, X.C., Xu, S.F., and Xu, M., (2015). Paclitaxel and etoposide co-loaded polymeric nanoparticles for the effective combination therapy against human osteosarcoma. Journal of nanobiotechnology, 13, p.22.

Zhang, Y., Yang, C., Wang, W., Liu, J., Liu, Q., Huang, F., Chu, L., Gao, H., Li, C., Kong, D., and Liu, Q., (2016). Co-delivery of doxorubicin and Curcumin by pH-sensitive prodrug nanoparticle for combination therapy of cancer. Scientific reports, 6, p. 21225.